Titanium isotopes as a tracer for the plume or island arc affinity of felsic rocks

Zhengbin Deng[1]*, Marc Chaussidon[1], Paul Savage[2], François Robert[3], Raphaël Pik[4], Frédéric Moynier[1, 5]

[1] Institut de Physique du Globe de Paris, Université Paris Diderot, Université Sorbonne Paris Cité, CNRS UMR 7154, 1 rue Jussieu, 75005, Paris, France.

[2] School of Earth and Environmental Sciences, University of St. Andrews, Irvine Building, St. Andrews, KY16 9AL, United Kingdom.

[3] Institut de Minéralogie, Physique des Matériaux et Cosmochimie, UMR 7590, Muséum National d'Histoire Naturelle, 75231 Paris Cedex 05, France.

[4] Centre de Recherches Pétrographiques et Géochimiques (CRPG), Université de Lorraine, CNRS UMR 7358, Vandoeuvre, France.

[5] Institut Universitaire de France, Paris, France.

*Corresponding author. Email: deng@ipgp.fr

Abstract

Indirect evidence for the presence of a felsic continental crust, such as the elevated $^{49}Ti/^{47}Ti$ ratios in Archean shales, has been used to argue for ongoing subduction at that time and therefore plate tectonics. However, rocks of intermediate to felsic compositions can be produced in both plume and island arc settings. The fact that Ti behaves differently during magma differentiation in these two geological settings might result in contrasting isotopic signatures. Here, we demonstrate that, at a given SiO_2 content, evolved plume rocks (tholeiitic) are more isotopically fractionated in Ti than differentiated island arc rocks (mainly calc-alkaline). We also show that the erosion of crustal rocks from whether plumes (mafic in average) or island arcs (intermediate in average) can all produce sediments having quite constant $^{49}Ti/^{47}Ti$ ratios being 0.1-0.3 per mille heavier than that of the mantle. This suggests that Ti isotopes are not a direct tracer for the SiO_2 contents of crustal rocks. Ti isotopes in crustal sediments are still a potential proxy to identify the geodynamical settings for the formation of the crust, but only if combined with additional SiO_2 information.

Keywords: titanium isotopes, plume, island arc, magma differentiation, plate tectonics

Significance Statement

The debate on the onset of plate tectonics in the Earth's history has partially originated from the controversial criteria of using felsic crust to trace plate tectonics in the past. Here we demonstrate how Ti isotope ratios can be used as a proxy for the affinity of felsic rocks to plume or island arc settings. Our study shows that, contrary to what was previously assumed, Ti isotopes cannot serve as a direct evidence for 3.5 Ga plate tectonics, but must be combined with other information on SiO_2 contents of crustal rocks to be reliable.

\body

Introduction

The onset of plate tectonics is still highly debated due to the fragmentary geologic record for the early Earth. The proposed onset time of plate tectonics in literature has ranged from > 4.2 Ga to 0.85 Ga, and the emergence of the felsic continental crust has been usually considered as a major proxy to trace plate tectonics in the past (*1-8*). Nonetheless, the validity of such a criteria to trace the onset of plate tectonics has been frequently questioned based on the fact that both plume (tholeiitic) and island arc (mainly calc-alkaline) settings are able to produce rocks of intermediate to felsic compositions (*9-11*). Thus, it is critical to find a geochemical proxy to differentiate the plume or island arc affinity of felsic rocks in the past.

Titanium isotopes have been recently proposed to be a direct tracer for the SiO_2 contents of crustal rocks, based on the monotonic correlation between the $\delta^{49}Ti$ values (the per mille deviation of the $^{49}Ti/^{47}Ti$ ratio relative to OL-Ti standard) and SiO_2 contents of differentiated island arc rocks (*1*). However, this proposal is yet to be confirmed since Ti isotopes can be expected to follow contrasting isotope systematics during magma differentiation in plume and island arc settings. For instance, plume lavas (H_2O-poor and reduced) have a higher solubility of Fe-Ti oxides than island arc lavas (H_2O-rich and oxidized), thus developing enrichments in both total Fe and TiO_2 contents during fractional crystallization of olivine and plagioclase (*12-14*), potentially leading to variable Ti isotopic fractionation of the melts during fractional crystallization of Fe-Ti oxides.

Here we report the Ti isotopic composition of a set of well-characterized rocks from two typical plume settings, the Hekla volcano in Iceland (*15*) and the Afar hotspot in East Africa (*16*). These data are compared to data from a typical arc setting (Agung volcano, Sunda Arc) (*17*), to establish the systematics for the isotopic behavior of Ti during magmatic differentiation. The Hekla/Afar and Agung rocks were chosen because they are good analogs to document the magmatic behaviors of Ti isotopes during the generation of the Archean crust. First, the ranges in major element composition for Hekla/Afar and Agung samples encompass the compositional ranges known for present-day plume and island arc settings, respectively (Fig. 1A). Second, rocks from Archean cratons have a TiO_2 versus MgO pattern similar to that shown by present day rocks from plume and island arc settings: tholeiitic rocks show an enrichment in TiO_2 during magma differentiation whereas calc-alkaline rocks do not (Fig. 1B). The systematics established for Ti isotopes in Hekla/Afar and Agung rocks allow to model $\delta^{49}Ti$ values of Archean crustal rocks from plume and island arc settings. These distributions are compared to Ti isotopic data on a large set of Archean sediments, *i.e.* banded iron formation (BIF), cherts and shales with ages from ≈ 3.8 Ga to ≈ 0.45 Ga, that were also studied, to identify the geodynamical origin of the Archean continental crust.

Results

The Hekla and Afar samples cover all the range in TiO_2 contents typical of Fe-Ti oxide fractionation in a plume setting (*15-16, 18*) (Fig. 1A). These samples are aphyric (< 5 % phenocryst), and show a wide lithological range from basalt to rhyolite with (i) progressive enrichments in SiO_2, K_2O, Rb and Th and (ii) progressive depletions in MgO, total Fe, CaO and TiO_2 contents (*15-16*). Their $\delta^{49}Ti$ values vary from −0.005 ± 0.028 ‰ to +2.012 ± 0.014 ‰. In addition, $\delta^{49}Ti$ values are strongly correlated with chemical parameters such as TiO_2, total Fe and SiO_2 contents (Figs. 2A-B). On the other hand, the $\delta^{49}Ti$ values of the Archean

BIFs, cherts and shales are less variable with values from +0.163 ± 0.028 ‰ to +0.500 ± 0.080 ‰ (Fig. 3A). These BIF, chert and shale samples are from rock formations that have been intensively studied (SI Appendix). Together with the Ti isotopic data for shales from literature (*1*), the present data confirm the systematically positive δ^{49}Ti values for sediments since early Archean (Fig. 3A). The majority of samples have δ^{49}Ti values of +0.079 ‰ to +0.366 ‰ (n = 88) with five samples showing values down to −0.018 ‰ or up to +0.791 ‰ (n = 5).

Discussion

The variations of δ^{49}Ti values in the Hekla/Afar samples are correlated with TiO_2, SiO_2 and total Fe in a manner indicating that they primarily reflect the fractional crystallization of Fe-Ti oxides during magma differentiation (Figs. 2A-B). The compositions of Agung samples from Sunda Arc (*17*, *19*) can be interpreted in the same way (Figs. 2A-B). However, while the end points of differentiation for Hekla/Afar and for Agung seem to be grossly similar in TiO_2 contents (Fig. 1A), the exact fractions of Ti remaining in the melt (f_Ti) at a given SiO_2 content are in fact very different for the two magmatic suites (at 60 wt% SiO_2 f_Ti ≈ 0.087 and ≈ 0.213 for Hekla/Afar and Agung, respectively; Fig. 2A). These fractions (f_Ti) can be estimated from the Ti/Rb ratio: Rb being strongly incompatible allows to correct for the change in TiO_2 content due to fractionation of Ti-free major silicate phases (see the inset in Fig. 1A). The fractional crystallization of ilmenite or titanomagnetite results in an increase of the δ^{49}Ti value of the melts (up to ≈ +2.012 ‰ for Hekla/Afar) during magma differentiation. Modeling of the correlation between δ^{49}Ti and f_Ti shows that the Ti isotopic fractionation between crystals (ilmenite or titanomagnetite) and melt (noted $\Delta^{49}Ti_{crystal\text{-}melt}$) increases during magma differentiation for the Hekla/Afar lavas (SI Appendix, Fig. S1), from ≈ −0.1 ‰ at ≈ 1500 K to ≈ −0.5 ‰ at ≈ 1150 K. This is likely not just due to a change in temperature but also to a change in melt structure with increasing SiO_2 contents, which results in an enhancement of the proportion of lower-coordinated Ti in silicate melts and of the Ti isotopic fractionation between oxides and melts. Hekla and Afar lavas follow very similar δ^{49}Ti-SiO_2 paths even though these two igneous suites have quite different peak TiO_2 contents (4.53 wt% for Hekla and 3.30 wt% for Afar). This confirms that the Ti stable isotopic behaviors during magma differentiation are primarily controlled by the f_Ti values but not the TiO_2 contents. While the Agung samples document a more limited compositional range (*17*), the calculated $\Delta^{49}Ti_{crystal\text{-}melt}$ value for these samples is similar to the values determined for the Hekla/Afar samples. The fundamental reason for the different δ^{49}Ti versus SiO_2 trends between plume and arc settings is that the plume lavas experience much larger fractionations of Ti after the saturation of Fe-Ti oxides due to (i) the lower fO_2 values delaying ilmenite or titanomagnetite saturation and allowing the enrichments of TiO_2 in magmas by olivine and plagioclase accumulation (*12*, *18*) (see the inset in Fig. 1B), and (ii) the higher TiO_2 contents in the magmas allowing larger magnitudes of fractionation of Ti by fractional crystallization of Fe-Ti oxides (*13*) (Fig. 2A). Therefore, the contrasting Ti stable isotopic behaviors between plume and island arc rocks suggest that Ti isotopes cannot be used as a direct tracer for the SiO_2 contents of the crustal protoliths of Archean sedimentary rocks contrary to recently proposed by (*1*). This is because δ^{49}Ti values in the range from ≈ 0.0 ‰ to ≈ +0.4 ‰ can be reached at very different SiO_2 contents on the plume and island arc trends (Fig. 2B). Ti isotopes are useful

to discriminate whether crustal rocks are from plume or island arc settings only when they reach δ^{49}Ti values ≥ 0.4 ‰, *i.e.* the felsic ends of the two trends (Fig. 2B).

It is worth noting that, despite being built on samples from present-day plume and island arc settings, the present δ^{49}Ti-SiO_2 proxy for the tholeiitic or calc-alkaline affinity of felsic rocks can be also applicable for Archean rocks. In the TiO_2 versus MgO plot (Fig. 1B), the rocks from Archean cratons exhibit magma differentiation paths very similar to those of present-day lavas, *i.e.* the enrichments of TiO_2 in plume-type (tholeiitic) rocks during the fractional crystallization of olivine and plagioclase, and the lack of such a TiO_2 enrichment in island arc-type (calc-alkaline) rocks (Fig. 1A). The Archean rocks only differ from the present-day lavas in a reduction of the maximum range in TiO_2 content, as a consequence of the higher degrees of mantle partial melting in the Archean (*20*). This is unlikely to significantly affect the isotopic behavior of Ti since the evolution of δ^{49}Ti values during magma differentiation is primarily controlled by the fraction of Ti remaining in the melt (f_Ti), as corroborated by the similar δ^{49}Ti-SiO_2 paths for Hekla and Afar igneous suites having quite different peak TiO_2 contents (Fig. 2).

While shales show high TiO_2 contents with an average value of ≈ 0.63 wt%, the BIFs and cherts are quite depleted in Ti with TiO_2 ≤ 0.01 wt% for the majority of samples (see the inset in Fig. 3A; Dataset S8). Such depletions in Ti for BIFs and cherts are the results of the enrichments of other elements during chemical precipitation processes (*e.g.* Si for cherts), thus modifying the proportions of detrital Fe-Ti oxides. Nonetheless, the δ^{49}Ti values of the present BIFs and cherts are similar to those of shales in this study and literature (*1*) (Dataset S7). The similar δ^{49}Ti between low- and high-TiO_2 sedimentary rocks confirms the robustness of Ti isotopes in tracing the composition of their protoliths. It is striking that the δ^{49}Ti values of BIFs, cherts and shales since 3.8 Ga have been rather uniformly 0.1-0.3 ‰ higher than the typical mantle value of ≈ 0 ‰ (*e.g.* mid-ocean ridge basalts, MORBs) (*17, 21*) with an average of +0.191 ± 0.013 ‰ (2se, n = 88) (*1*). This can however be simply explained from considerations on the likely distributions of δ^{49}Ti values in plume and island arc rocks. These distributions can be modeled in Fig. 3B from the distribution of SiO_2 contents (extracted from the GeoRoc database; SI Appendix, Fig. S2) and from the relation established between SiO_2 and δ^{49}Ti (Fig. 2B). While both plume (in average SiO_2 ≈ 50 wt%) and island arc settings (in average SiO_2 ≈ 59 wt%), and Archean tonalite-trondhjemite-granodiorite rocks (TTGs) or Paleozoic granites with SiO_2 ≈ 65-70 wt% (Dataset S6) (*1*), can develop δ^{49}Ti values close to the values of Archean sedimentary rocks. Thus, the uniform δ^{49}Ti value of Archean sediments at ≈ +0.2 ‰ is not a solid argument for the presence of an early Archean felsic continental crust. Future studies of Archean sediments should aim at combining Ti isotopes with reliable information of SiO_2 contents of their protoliths, in order to differentiate safely a plume from an island arc affinity of the continental crust in the past. For instance, since the modern continental crust is known to be in average "andesitic" in bulk composition, *i.e.* SiO_2 = 60.6 wt% with SiO_2 = 63.5-66.6 wt% for its middle to upper parts (*22*), the δ^{49}Ti values of +0.1-0.3‰ for the Phanerozoic sedimentary rocks likely suggest an island arc origin of this continental crust.

Materials and Methods

The Hekla/Afar and sedimentary samples were crushed into powders with an agate mortar, and the rock powders were dissolved by HF-HNO_3 digestion on a hotplate or by alkali fusion (*15*, *23*). Sample aliquots were mixed with a ^{47}Ti-^{49}Ti double spike, and were processed with a three-step ion-exchange chromatographic procedure, consisting of Eichrom DGA and Bio-Rad AG1-X8 resins (*24*), to purify Ti from the matrices. Ti isotopes were measured on a Thermo-Fisher Neptune Multi-Collector Inductively-Coupled-Plasma Mass-Spectrometer (MC-ICP-MS) at the Institut de Physique du Globe de Paris with medium mass resolution ($M/\Delta M \approx 5800$). Samples were introduced in 0.5 M HNO_3 + 0.0015 M HF through an Apex desolvating nebulizer with a concentration of 300 ppb Ti. Signals of ^{46}Ti, ^{47}Ti, ^{48}Ti and ^{49}Ti were used for double spike inversion using the IsoSpike software (*25*).

Full Methods and associated references are available in SI Appendix of the online version.

References:

1. Greber ND *et al.* (2017) Titanium isotopic evidence for felsic crust and plate tectonics 3.5 billion years ago. *Science* **357**: 1271–1274. doi: 10.1126/science.aan8086
2. Korenaga J (2013) Initiation and evolution of plate tectonics on Earth: theories and observations. *Annu. Rev. Earth Planet. Sci.* **41**: 117–151. doi: 10.1146/annurev-earth-050212-124208
3. Watson EB, Harrison TM (2005) Zircon thermometer reveals minimum melting conditions on earliest Earth. *Science* **308**: 841–844. doi: 10.1126/science.1110873
4. Martin H (1986) Effect of steeper Archean geothermal gradient on geochemistry of subduction-zone magmas. *Geology* **14**: 753–756. doi: 10.1130/0091-7613(1986)14<753:EOSAGG>2.0.CO;2
5. Dhuime B, Wuestefeld A, Hawkesworth CJ (2015) Emergence of modern continental crust about 3 billion years ago. *Nat. Geosci.* **8**: 552−555. doi: 10.1038/ngeo2466
6. Tang M, Chen K, Rudnick RL (2016) Archean upper crust transition from mafic to felsic marks the onset of plate tectonics. *Science* **351**: 372−375. doi: 10.1126/science.aad5513
7. Harrison TM, Bell EA and Boehnke P (2017) Hadean zircon petrochronology. *Rev. Mineral. Geochem.* **83**: 329–363. doi: 10.2138/rmg.2017.83.11
8. Boehnke P, Bell EA, Stephan T, Trappitsch R, Keller CB, Pardo OS, Davis AM, Harrison TM, Pellin MJ (2018) Potassic, high-silica Hadean crust. *Proc. Natl. Acad. Sci. USA*, p.201720880. doi: 10.1073/pnas.1720880115
9. Campbell IH, Davies DR (2017) Raising the continental crust. *Earth Planet. Sci. Lett.* **460**: 112–122. doi: 10.1016/j.epsl.2016.12.011
10. Reimink JR, Chacko T, Stern RA, Heaman LM (2014) Earth's earliest evolved crust generated in an Iceland-like setting. *Nat. Geosci.* **7**: 529–533. doi: 10.1038/ngeo2170
11. Willbold M, Hegner E, Stracke A, Rocholl A (2009) Continental geochemical signatures in dacites from Iceland and implications for models of early Archaean crust formation. *Earth Planet. Sci. Lett.* **279**: 44–52. doi: 10.1016/j.epsl.2008.12.029
12. Toplis MJ, Carroll MR (1995) An experimental study of the influence of oxygen fugacity on Fe-Ti oxide stability, phase relations, and mineral-melt equilibria in ferro-basaltic systems. *J. Petrol.* **36**: 1137–1170. doi: 10.1093/petrology/36.5.1137
13. Cawthorn RG, Biggar GM (1993) Crystallization of titaniferous chromite, magnesian

ilmenite and armalcolite in tholeiitic suites in the Karoo Igneous Province. *Contrib. Mineral. Petrol.* **114**: 221–235. doi: 10.1007/BF00307757
14. Nandedkar RH, Ulmer P, Müntener O (2014) Fractional crystallization of primitive, hydrous arc magmas: an experimental study at 0.7 GPa. *Contrib. Mineral. Petrol.* **167**: 1015. doi: 10.1007/s00410-014-1015-5
15. Savage PS, Georg RB, Williams HM, Burton KW, Halliday AN (2011) Silicon isotope fractionation during magmatic differentiation. *Geochim. Cosmochim. Acta*. **75**: 6124–6139. doi: 10.1016/j.gca.2011.07.043
16. Pik R, Marty B, Hilton DR (2005) How many mantle plumes in Africa? The geochemical point of view. *Chem. Geol.* **226**: 100–114. doi: 10.1016/j.chemgeo.2005.09.016
17. Millet MA, Dauphas N, Greber ND, Burton KW, Dale CW, Debret B, Macpherson CG, Nowell GM, Williams HM (2016) Titanium stable isotope investigation of magmatic processes on the Earth and Moon. *Earth Planet. Sci. Lett.* **449**: 197–205. doi: 10.1016/j.epsl.2016.05.039
18. Prytulak J, Elliott T (2007) TiO_2 enrichment in ocean island basalts. *Earth Planet. Sci. Lett.* **263**: 388–403. doi: 10.1016/j.epsl.2007.09.015
19. Dempsey S (2013) Geochemistry of volcanic rocks from the Sunda Arc. *Doctoral thesis*, Durham University.
20. Keller CB, Schoene B (2012) Statistical geochemistry reveals disruption in secular lithospheric evolution about 2.5 Gyr ago. *Nature* **485**: 490–493. doi: 10.1038/nature11024
21. Deng Z, Moynier F, Sossi PA, Chaussidon M (in press) Bridging the depleted MORB mantle and the continental crust using titanium isotopes. *Geochem. Perspect. Lett.*
22. Rudnick RL, Gao S (2003) Composition of the continental crust. *Treatise on Geochemistry* **3**: 659. doi: 10.1016/B0-08-043751-6/03016-4
23. Deng Z, Moynier F, van Zuilen K, Sossi PA, Pringle EA, Chaussidon M (2018) Lack of resolvable titanium stable isotopic variations in bulk chondrites. *Geochim. Cosmochim. Acta*. **239**: 409–419. doi: 10.1016/j.gca.2018.06.016
24. Zhang J, Dauphas N, Davis AM, Pourmand A (2011) A new method for MC-ICPMS measurement of titanium isotopic composition: Identification of correlated isotope anomalies in meteorites. *J. Anal. At. Spectrom.* **26**: 2197–2205. doi: 10.1039/C1JA10181A
25. Creech JB, Paul B (2015) IsoSpike: Improved Double‐Spike Inversion Software. *Geostand. Geoanal. Res.* **39**: 7−15. doi: 10.1111/ j.1751-908X.2014.00276.x

Acknowledgments

General:

We thank Pascale Louvat, Jessica Dallas and Pierre Burckel for the maintenance of the (MC)-ICP-MS at IPGP, and John Creech for providing updated IsoSpike. Paolo Sossi and Kirsten van Zuilen are appreciated for discussions. The editor and two anonymous reviewers are thanked for the comments, which significantly improve this manuscript.

Funding:

FM acknowledges funding from the European Research Council under the H2020 framework program/ERC grant agreement #637503 (Pristine). FM and MC thank the financial support of the UnivEarthS Labex program at Sorbonne Paris Cité (ANR-10-LABX-0023 and ANR-11-IDEX-0005-02). Parts of this work were supported by IPGP multidisciplinary program PARI, and by Region Île-de-France SESAME Grant no. 12015908.

Author contributions:

Z.D., M.C. and F.M. designed the project; P.S., F.R. and R.P. provided the samples for study; Z.D. performed the research and analyzed the data; and Z.D., M.C. and F.M. wrote the paper, and P.S., F.R. and R.P. participated in discussions and commented on the paper.

Competing interests:

The authors declare no conflict of interest.

Figure 1:

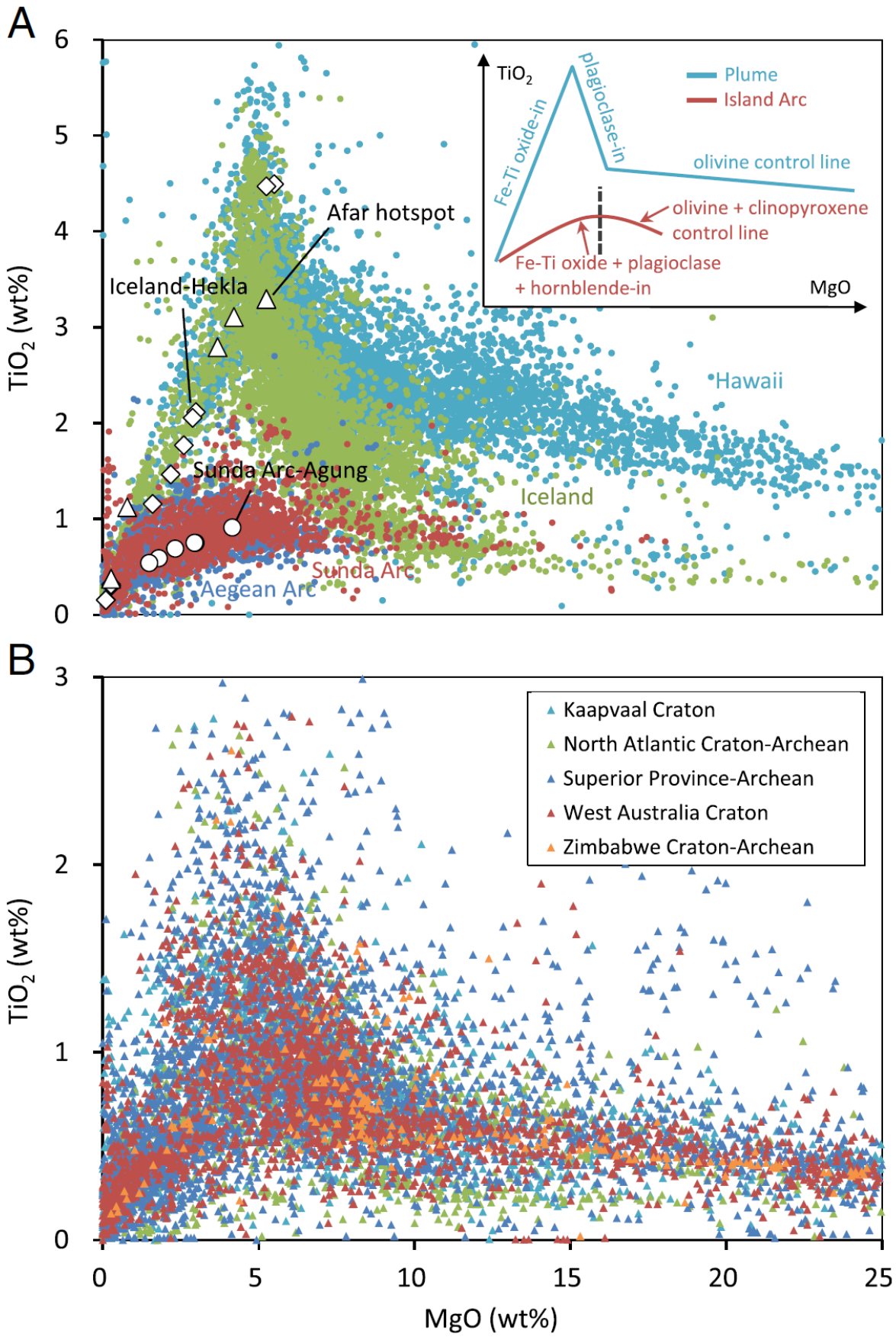
A
B
TiO2 (wt%)
MgO (wt%)
Afar hotspot
Iceland-Hekla
Sunda Arc-Agung
Aegean Arc
Sunda Arc
Iceland
Hawaii
TiO2
MgO
Fe-Ti oxide-in
plagioclase-in
olivine control line
olivine + clinopyroxene
control line
Fe-Ti oxide + plagioclase
+ hornblende-in
Plume
Island Arc
Kaapvaal Craton
North Atlantic Craton-Archean
Superior Province-Archean
West Australia Craton
Zimbabwe Craton-Archean

Figure 2:

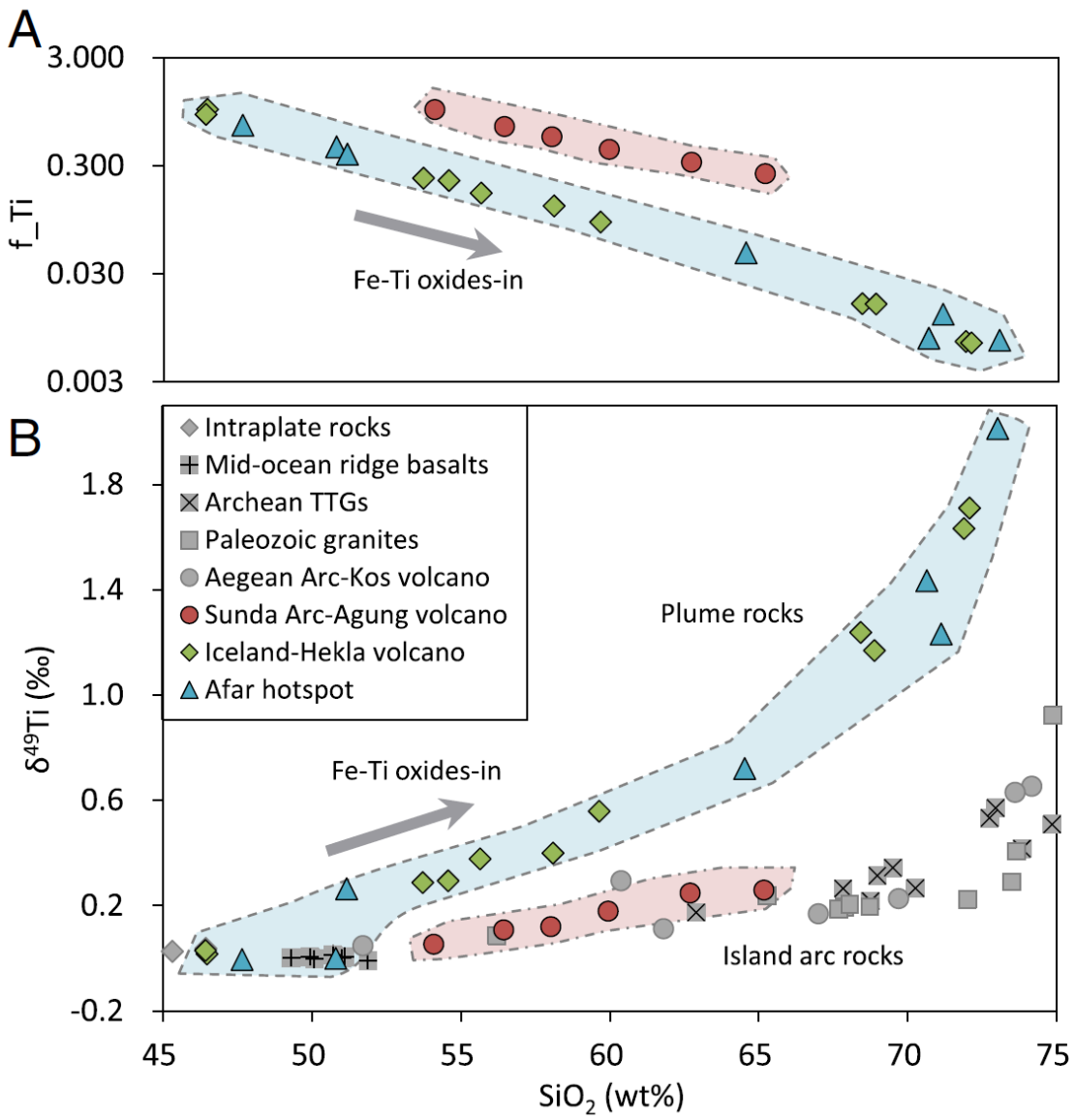
A
3.000
0.300
0.030
0.003
f_Ti
Fe-Ti oxides-in
B
Intraplate rocks
Mid-ocean ridge basalts
Archean TTGs
Paleozoic granites
Aegean Arc-Kos volcano
Sunda Arc-Agung volcano
Iceland-Hekla volcano
Afar hotspot
Plume rocks
Fe-Ti oxides-in
Island arc rocks
1.8
1.4
1.0
0.6
0.2
-0.2
δ49Ti (‰)
45
50
55
60
65
70
75
SiO2 (wt%)

Figure 3:

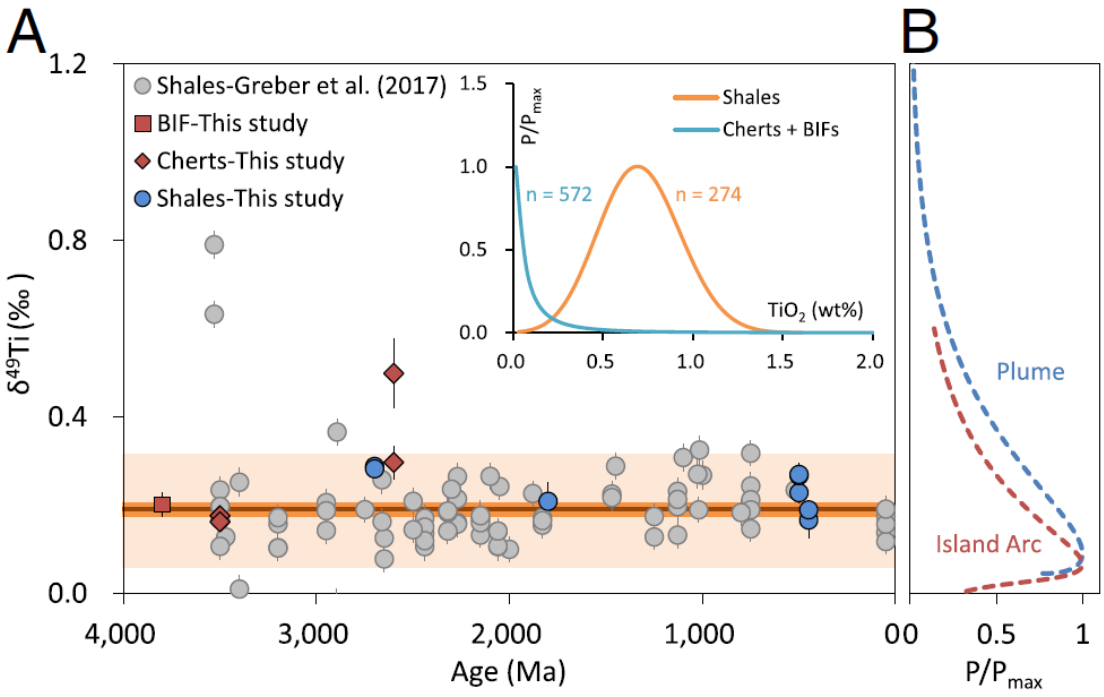
A
B
1.2
0.8
0.4
0.0
δ49Ti (‰)
Shales-Greber et al. (2017)
BIF-This study
Cherts-This study
Shales-This study
1.5
1.0
0.5
0.0
P/Pmax
Shales
Cherts + BIFs
n = 572
n = 274
TiO2 (wt%)
0.0
0.5
1.0
1.5
2.0
Plume
Island Arc
4,000
3,000
2,000
1,000
0
Age (Ma)
0
0.5
1
P/Pmax

Figure captions

Fig. 1. The TiO_2 and MgO contents in the rocks from **(A)** present-day plume (Iceland and Hawaii) and island arc (Sunda and Aegean Arcs) settings, and from **(B)** Archean cratons. The chemical composition data of these rocks are from the GeoRoc database. The samples from Hekla (Iceland) (*15*), Afar hotspot (East Africa) and Agung (Sunda Arc) (*19*) are shown in **(A)**. The inset in **(A)** illustrates the typical fractionation path inducing the TiO_2 variations in plume lavas (*18*) and island arc lavas (*14*).

Fig. 2. (A) the fractions of Ti (f_Ti) remaining in the melts versus SiO_2 contents and **(B)** the variations of δ^{49}Ti values versus SiO_2 contents, for the Hekla (*15*), Afar hotspot (East Africa) and Agung (*17*, *19*) samples. The f_Ti values of the samples were estimated from their Ti/Rb ratios. The arrows indicate the effects from the fractional crystallization of Fe-Ti oxides, *e.g.* ilmenite, titanomagnetite or titanite (*14*, *18*). Literature data of Paleozoic granites, Archean tonalite-trondhjemite-granodiorite rocks (TTGs) and volcanic rocks from the Kos volcano of Aegean Arc in (*1*), as well as those of mid-ocean ridge basalts (MORBs) and intraplate rocks in (*17*), are also shown for comparison. The errors on the δ^{49}Ti values are 95 % confidence intervals (95% c.i.) that are smaller than the size of the labels.

Fig. 3. (A) The δ^{49}Ti values of Archean BIF, cherts and shales versus depositional ages, and previous data for shales (*1*) (Dataset S7). The dark orange line shows the average δ^{49}Ti value of ≈ +0.191 ‰ for the present data with the orange and light orange areas showing 2se (±0.013 ‰) and 2sd (±0.119 ‰) of these data, respectively. The inset shows the distribution of the literature TiO_2 contents in BIFs, cherts and shales with the probabilities normalized to the maximal probability (P/P_{max}) (Dataset S8). **(B)** Distribution of the δ^{49}Ti values for plume and island arc rocks in the GeoRoc database. The samples were compiled into groups in each 0.5 wt% SiO_2 interval following Gaussian distribution (SI Appendix, Fig. S2). This SiO_2 distribution was further translated into the δ^{49}Ti density based on the δ^{49}Ti-SiO_2 systematics for plume settings (this study) and island arc settings (*1*).

Supporting Information (SI) for

Titanium isotopes as a tracer for the plume or island arc affinity of felsic rocks

Zhengbin Deng*, Marc Chaussidon, Paul Savage, François Robert, Raphaël Pik, Frédéric Moynier

*Correspondence to: deng@ipgp.fr

This PDF file includes:

Materials and Methods
Supplementary Text
Figs. S1 to S2
References 26-50

Other Supporting Information (SI) for this manuscript includes the following:

Datasets S1 to S8 (separate files)

Materials

Hekla volcanic samples

The Hekla volcanic samples were collected from the flow cores of the historic eruptions of the Hekla volcano, and detailed information on these samples have been published elsewhere (*15*). These rocks cover a compositional range from basaltic to rhyolitic (Dataset S4), and are predominantly aphyric with < 5 % phenocryst contents, which ensure their capability to reflect the melt compositions during magma differentiation. Eleven samples, including two basalt ("HEK05-09" and "HEK12-09"), three basaltic andesite ("HEK-14-09", "HEK17-09" and "HEK21-09"), two andesite ("HEK11-09" and "HEK15-09"), two dacite ("HEK18-9" and "HEK19-09") and two rhyolite ("HEK01-10" and "HEK03-10"), were selected to study their Ti isotopic composition (Dataset S2). The same samples have been previously studied for the stable isotopic compositions of Mo (*26*), Zn (*27*), Si (*15*) and V (*28*). While Mo, Zn and Si have limited isotopic variations over the composition range from basaltic to rhyolitic, V is characterized by a progressive enrichment of the heavy isotope during fractional crystallization of Fe-Ti oxides (≈ 1.5 ‰/amu) (*28*). A similar collection of Hekla samples

has been also studied for the Fe isotopic compositions (29): this showed an evolution in two steps for Fe isotopic compositions during magma differentiation, i.e., negligible Fe isotopic variations when SiO_2 = 45-65 wt% and a slight enrichment in the heavy Fe isotopes when SiO_2 > 65 wt%.

The studies on the olivine-hosted melt inclusions from the eruptions of Hekla volcano show that, although experiencing some degrees of syn-eruptive degassing, the Hekla magmas are generally volatile-undersaturated before the eruptions, H_2O being the major volatile species (*30*). H_2O behaves as an incompatible component during magma differentiation in the Hekla volcano with H_2O from ≈ 0.80 wt% in the basaltic andesites to ≈ 5.67 wt% in the rhyolites, with a relatively constant H_2O/K_2O ratio of ≈ 2 (*30*, *31*). The estimate for the magma chamber depth using vapor saturation pressures and phenocryst assemblages suggests a crustal magma storage at ≈ 7 km (*30*) and ≈ 6 km (*32*), respectively. Such a crustal magma storage depth at ≈ 6-7 km for the Hekla volcano contrasts with the much shallower magma storage depths for the volcanoes in the Sunda Arc, e.g., Agung (≈ 1.9 km), Sinabung (≈ 0.9 km), Kerinci (≈ 0.7 km), Slamet (≈ 1.2 km), Lawu (≈ 1.1 km), Lamongan (≈ 3.4 km) and Anak Krakatau (≈ 0.7 km) (*33*).

Afar volcanic samples

The Afar samples were collected from the Stratoid Series in the Afar hotspot from East Africa (*16*), including basalt ("AF13-46", "AF13-34" and "AF13-35"), dacite ("AF15-17") and rhyolite ("AF15-40", "AF15-10" and "AF15-11"). These lavas cover the eruption ages ranging between ≈ 4 and ≈ 1 Ma (unpublished data from Pik). The Afar lavas also exhibit the enrichment of TiO_2 during the magma differentiation before the saturation of Fe-Ti oxides. However, in detail the highest TiO_2 content of the Afar lavas is 3.30 wt%, which is much lower than the highest TiO_2 content (4.53 wt%) among the Hekla lavas (Dataset S4). Once the magmas reach the saturation of Fe-Ti oxides, the TiO_2 contents of the magmas decrease with the progressive depletions of total Fe, MgO and CaO (Dataset S4).

Shale samples

The shale samples are from the Canadian Shield and Quebec Appalachians (*34*). Samples "Y-47-83" and "3-05-84" are from the late Archean Gilman Formation and Malartic Group (≈ 2.7 Ga), respectively, in the Abitibi green belt. Sample "85-RG-17-A" is from the mid-Proterozoic Baby Group (≈ 1.8 Ga), Labrador Through. While samples "113", "30" and "43" were collected from the Cambrian to Early Ordovician Magog, St-Roch and Armagh Groups (≈ 0.5 Ga), respectively, samples "PEL 17" and "PEL14" are from the Late Ordovician to Early Silurian Cabano and St-Léon Formations (≈ 0.45 Ga) in the Appalachian Belt (Dataset S3) (*34*).

Banded iron formation (BIF) samples

Sample "sjm/gr/97/21" was a BIF enclave collected from the Amîtsoq gneisses in southern West Greenland (Dataset S3). The gneiss complex from the nearby Akilia Island has been intruded by a metamorphosed quartz-dioritic dike with a zircon U-Pb age of 3,860 ± 10

Ma (*35*, *36*), which confirms the depositional age of the BIF sample in this study at or before ≈ 3.8 Ga.

Chert samples

Sample "2 of 16-09-65" is from the Onverwacht Group, Barberton Greenstone Belt (South Africa) (Dataset S3). The dacitic tuffs of the Onverwacht Group yield the $^{207}Pb/^{206}Pb$ single zircon evaporation ages between 3,445 ± 3 and 3,416 ± 5 Ma (*37*), implying that sample "2 of 16-09-65" has a deposited age of ≈ 3.5 Ga.

Sample "PPRG 006" was collected from the Warrawoona Formation, Pilbara Block in Western Australia (Dataset S3) (*38*). The dacite in the Warrawoona Formation has a zircon U-Pb age of 3,452 ± 16 Ma (*39*).

Sample "SBO 297" is from the Ventersdorp Supergroup in central South Africa (Dataset S3), which has been previously studied for O isotopic compositions (*40*). The direct dating of the stromatolitic limestones provides an isochron age of 2,557 ± 49 Myrs for the Schmidtsdrif Formation within the Ventersdorp Supergroup (*41*).

Sample "PPRG 226" was collected from the Manjeri Formation, Belingwe Greenstone Belt (Zimbabwe) (Dataset S3) (*42*). The Pb-Pb isochrons from stromatolitic limestones from the Manjeri Formation yield an age of 2,706 ± 49 Ma (*43*).

Methods

Sample preparation and digestion

The rock specimens of the Hekla/Afar volcanic rocks, shales and cherts were washed to remove the soil or organic components. The samples were crushed and further powdered in an agate mill (*15*). Around 30-60 mg of sample powder of Hekla/Afar samples and rock standards (BIR-1, BHVO-2, BCR-2 and AGV-1) were dissolved in the 7 ml Savillex PFA beakers using 2 ml 26 M HF and 1 ml 16 M HNO_3 for overnight cold reaction at room temperature. Afterwards, the samples were dried, and were dissolved in 2 ml 26 M HF and 1 ml 16 M HNO_3 on hot plate at 100 °C for three days. These samples were dried again, and the sample residuals were dissolved in 3 ml 6 M HCl at 130 °C to decompose the fluorides forming during sample digestion by HF. By comparison, around 510-850 mg of powder of chert samples were dissolved following similar protocols but using twice much volumes of 26 M HF and 16 M HNO_3 acids on hot plate at 120 °C for seven days.

The shale samples were dissolved by alkali fusion following the protocol in (*15*) and (*44*). About 17-37 mg of sample powder was fused in Ag crucibles with addition of 200 mg NaOH pellets (99.99 % trace metal basis, Sigma Aldrich Company). The fusion was carried out in a furnace at 720 °C for 15 min, and the fused samples were dissolved in 1 M HNO_3. To ensure that the Ti isotopic measurements of the Hekla samples are not affected by digestion methods, two Hekla samples ("HEK15-09" and "HEK03-10") were digested by alkali fusion to compare with the aliquots dissolved by HF-HNO_3 acids (Dataset S2).

Chromatographic Ti purification

Before the purification of Ti, the sample solutions were mixed with proper amounts of ^{47}Ti-^{49}Ti double spike. The mixture was heated on a hot plate at 100 °C for > 1 h to ensure the homogenization between sample and double spike. The purification of Ti followed a three-steps procedure revised after (*23, 24*): (i) the samples were loaded on a column of 1.1 cm^3 Bio-Rad AG1-X8 resin (200-400 meshes) in 0.5 ml 6 M HCl, and Ti was collected with matrix elements except Fe in 6 ml 6M HCl; (ii) the Ti cut was dissolved in 100 µl 12 M HNO_3, and loaded on a column with 0.2 cm^3 Eichrom DGA resin with particle size of 50-100 µm. Then the matrix elements were washed out by addition of 900 µl 12 M HNO_3. Subsequently, the Ti was collected by washing with 600 µl MilliQ H_2O and (iii) the Ti cuts from the last step were loaded on the AG1-X8 columns again with 0.5 ml 4 M HF, and the remaining matrix elements were washed out by 9.5 ml 4 M HF. The Ti of the samples was finally collected with additional 5 ml 6 M HCl + 0.01 M HF.

Ti standards and ^{47}Ti-^{49}Ti double spike

A Ti reference material (hereafter expressed as IPGP-Ti) was made from a Ti ICP standard solution (1000 µg/ml PlasmaCal, SCP Science, Lot SC7186430). A ^{47}Ti-^{49}Ti double spike was prepared by mixing enriched ^{47}Ti (95.7 %) and ^{49}Ti (93.3 %), which were purchased from CortecNet (Voisins-le-Bretonneux, France), and was then stored in 1 M HNO_3 + 0.01 M HF. The optimization mixing ratio between sample and double spike was determined using the toolbox from (*45*). The IPGP-Ti and the ^{47}Ti-^{49}Ti double spike were measured separately on mass spectrometer to estimate their Ti isotopic compositions. Cr was doped to determine the instrumental mass bias on Cr isotopes by normalizing to a natural ^{53}Cr/^{52}Cr ratio of 0.1134 (*46*). Once the instrumental ^{50}Cr$^+$/^{52}Cr$^+$ ratio was obtained, the isobaric interferences of ^{50}Cr$^+$ on ^{50}Ti$^+$ can be corrected through monitoring the intensities of ^{52}Cr$^+$ on mass spectrometer. Afterwards, nine aliquots of IPGP-Ti with increasing proportions of double spike were measured. The $\delta^{49}Ti_{IPGP\text{-}Ti}$ value of IPGP-Ti can be preliminarily calculated by conducting double spike inversion for the Ti isotopic data of these mixtures, and the isotopic composition of the ^{47}Ti-^{49}Ti double spike can be further obtained by mass-dependently adapting the calculated $\delta^{49}Ti_{IPGP\text{-}Ti}$ value for IPGP-Ti to 0 ‰. The optimized mixing ratios between IPGP-Ti and double spike were ranging from 0.42 to 0.60 based on the calibration.

Measurements by mass spectrometry, data reduction and results

The Ti cuts were introduced into the Neptune MC-ICP-MS housed at IPGP by using 0.5 M HNO_3 + 0.0015 M HF. An APEX HF desolvating nebulizer (Elemental Scientific Inc., USA) was used to enhance the sensitivity. The typical sensitivities on the MC-ICP-MS were 17-19 V on ^{48}Ti$^+$ when using a 10^{11} Ω resistor and a Ti concentration of 300 ppb under medium mass resolution ($M/\Delta M \approx 5800$). The OL-Ti standard was calibrated relative to the IPGP-Ti standard used in (*17*) and (*1*), which provide a $\delta^{49}Ti_{IPGP\text{-}Ti}$ value of −0.140 ± 0.011 ‰ (95 % c.i., n = 8) for IPGP-Ti standard. After each analysis, a washing of the sampling tube and the Apex HF desolvating nebulizer was conducted in two steps, i.e. a first rinse with 1.2 M HNO_3 + 0.0015 M HF and a second rinse with 0.5 M HNO_3 + 0.0015 M HF. Each step of washing contains 50 cycles with an integration time of 8 s, and after the washing the typical background on ^{48}Ti$^+$ was 2-5 mV.

The intensities on $^{44}Ca^+$, $^{46}Ti^+$, $^{47}Ti^+$, $^{48}Ti^+$ and $^{49}Ti^+$ were measured simultaneously. Each analysis consisted of 100 cycles with an integration time of 8 s. The intensities on $^{44}Ca^+$ were used to correct the interferences of $^{46}Ca^+$ and $^{48}Ca^+$ on $^{46}Ti^+$ and $^{48}Ti^+$, respectively. Since Ca isotopes can be fractionated on the MC-ICP-MS, the natural Ca isotopic ratios cannot be directly used to correct for the interferences of Ca on Ti. Alternatively, the instrumental Ca isotopic ratios were estimated by mass-dependently fractionate the natural Ca isotopic abundances ($^{44}Ca/^{46}Ca$ = 657.03 and $^{44}Ca/^{48}Ca$ = 11.14) (*24*) with the instrumental mass fractionation factor of Ti. The estimated instrumental $^{44}Ca/^{46}Ca$ and $^{44}Ca/^{48}Ca$ ratios were then applied to correct for the interferences of $^{46}Ca^+$ and $^{48}Ca^+$ on $^{46}Ti^+$ and $^{48}Ti^+$, respectively. Due to the use of a quartz-made injector, there can be also molecular isobaric interferences from silicon oxides and fluorides on the isotopes of Ti, such as $^{28}Si^{16}O^+$, $^{30}Si^{16}O^+$ and $^{28}Si^{19}F^+$. These interferences were avoided by measuring the intensities of $^{44}Ca^+$, $^{46}Ti^+$ and $^{47}Ti^+$ on the lower masses of mass 44, 46 and 47. While the molecular interferences of $^{29}Si^{19}F^+$ and $^{30}Si^{19}F^+$ on $^{48}Ti^+$ and $^{49}Ti^+$, respectively, are negligible, the intensities of $^{48}Ti^+$ and $^{49}Ti^+$ were measured on the central masses of mass 48 and 49.

The data reduction was carried out by using the IsoSpike software developed by (*25*). The intensities of ^{46}Ti, ^{47}Ti, ^{48}Ti and ^{49}Ti after the correction of Ca isobaric interferences were used for double spike inversion to determine the Ti isotopic composition of the samples. The data can be normalized as δ-notation relative to OL-Ti standard:

$$d^{49}Ti_{OL\text{-}Ti} = \left[\frac{\left({}^{49}Ti / {}^{47}Ti \right)_{sample}}{\left({}^{49}Ti / {}^{47}Ti \right)_{OL\text{-}Ti}} - 1 \right] \times 1000 \qquad \text{(Eq. 1)}$$

In order to facilitate data comparison in the community, the present data are reported as $\delta^{49}Ti_{OL\text{-}Ti}$ values, i.e. $\delta^{49}Ti$ if not specifically clarified later. For the rock standards including BHVO-2, BIR-1, BCR-2 and AGV-1, the measurement precisions are the 95 % confidence intervals (95 % c.i.) of three to sixteen duplicates for each sample, which are ≤ 0.022 ‰.

The calibration shows that the IPGP-Ti standard has a $\delta^{49}Ti$ value of +0.140 ± 0.011 ‰ (n = 8). The measurements of a spiked IPGP-Ti aliquot after the DGA pass against the un-cleaned spiked IPGP-Ti provide a systematically resolvable $\Delta^{49}Ti$ value of +0.022 ± 0.009 ‰ (n = 9). This small drift is due to the presence of the highly isotopically fractionated Ca in the used double spike. Since all the samples have been measured against the un-cleaned spiked IPGP-Ti standard, a correction on all the data with error propagation was conducted to take into account this effect, allowing a high-precision inter-laboratory data comparison in the future. After the correction, the $\delta^{49}Ti$ values for rock standards BIR-1, BHVO-2, BCR-2 and AGV-1 are consistent with those reported by (*47*) and (*17*) within errors (Dataset S1). Furthermore, the two alkali fusion aliquots of samples HEK15-09 and HEK03-10 show consistent $\delta^{49}Ti$ values with those of the HF-HNO_3 dissolution aliquots within an analytical precision of 0.030 ‰ (Dataset S2). This consistency implies that the Ti isotopic measurements in this study are not affected by the sample dissolution methods.

Supplementary Text

Mechanisms inducing Ti isotopic variations during magma differentiation

The igneous rocks from both plume and island arc settings become isotopically heavier in Ti with increasing SiO_2 (Fig. 2B). These Ti isotopic variations are intimately associated with the significant decreases of TiO_2 and total Fe (Fig. 2A; Datasets S2 and S4-S5). Such a correlation indicates that the observed Ti isotopic variations here are mainly controlled by the fractional crystallization of Fe-Ti oxides (*17*). Ti is present as 6-folded coordination in Fe-Ti oxides (*48*), while it can be 4-, 5- or 6-fold coordinated in silicate melts (*49*). Given a similar metal-ligand environment (Ti-O), the heavier Ti isotopes would preferentially enter the lower coordinated sites. This predicts that Fe-Ti oxides would be more enriched in the lighter Ti isotopes than silicate melts during fractional crystallization, and the removal of Fe-Ti oxides leaves behind a residual magma isotopically heavy in Ti.

In this process, two parameters control the evolution of the δ^{49}Ti values of the melt, i.e., the crystal-melt Ti isotopic fractionation factor ($a^{49/47}_{crystal\text{-}melt\_i\_or\_j} = R^{49/47}_{crystal} / R^{49/47}_{melt\_i\_or\_j}$) and the fraction of Ti ($f\_Ti_{melt\_j}$ and $f\_Ti_{melt\_i}$) remaining in melt j and melt i compared to the parental melt. The mass balance equation can be written as:

$$R^{49/47}_{melt\_i} = R^{49/47}_{0} \cdot \left(f\_Ti_{melt\_i}\right)^{a^{49/47}_{crystal\text{-}melt\_i} - 1} \quad \text{(Eq. 2)}$$

$$R^{49/47}_{melt\_j} = R^{49/47}_{0} \cdot \left(f\_Ti_{melt\_j}\right)^{a^{49/47}_{crystal\text{-}melt\_j} - 1} \quad \text{(Eq. 3)}$$

with $R^{49/47}_{0}$, $R^{49/47}_{melt\_i}$ and $R^{49/47}_{melt\_j}$ the ^{49}Ti/^{47}Ti ratios of the parental melt, melt i and melt j, respectively. The isotopic difference between melt j and melt i can be expressed as:

$$\frac{R^{49/47}_{melt\_j}}{R^{49/47}_{melt\_i}} = \frac{\left(f\_Ti_{melt\_j}\right)^{a^{49/47}_{crystal\text{-}melt\_j} - 1}}{\left(f\_Ti_{melt\_i}\right)^{a^{49/47}_{crystal\text{-}melt\_i} - 1}} \quad \text{(Eq. 4).}$$

When melt j is compositionally very close to melt i, and melt j and melt i have quite similar liquidus temperatures, $a^{49/47}_{crystal\text{-}melt\_j}$ is approximately equal to $a^{49/47}_{crystal\text{-}melt\_i}$. As such, Equation 4 can be simplified into:

$$\frac{R^{49/47}_{melt\_j}}{R^{49/47}_{melt\_i}} \approx \left(\frac{f\_Ti_{melt\_j}}{f\_Ti_{melt\_i}}\right)^{a^{49/47}_{crystal\text{-}melt\_j} - 1} \quad \text{(Eq. 5).}$$

In delta notation, Equation 5 writes:

$$\Delta^{49}Ti_{melt\_j\text{-}melt\_i} = \delta^{49}Ti_{melt\_j} - \delta^{49}Ti_{melt\_i} \approx 1000 \times \left(\alpha^{49/47}_{crystal\text{-}melt\_j} - 1\right) \times \ln\left(\frac{f\_Ti_{melt\_j}}{f\_Ti_{melt\_i}}\right) \quad \text{(Eq. 6)}$$

The derivation of Equation 6 can provide the instant crystal-melt Ti isotopic fractionation factor $\Delta^{49}Ti_{crystal\text{-}melt} = 1000 \times \left(\alpha^{49/47}_{crystal\text{-}melt} - 1\right)$. In fact, $f\_Ti_{melt\_j}$ or $f\_Ti_{melt\_i}$ can be estimated by comparing the Ti/Rb ratios of the samples to account for the variations of TiO_2 contents due to fractional crystallization of (i) Ti-free minerals (e.g., olivine and plagioclase) and (ii) Ti-bearing minerals (e.g., pyroxene, ilmenite and titanomagnetite) (see the inset in Fig. 1A) (*14*, *18*). As shown in Fig. S1, the $\Delta^{49}Ti_{crystal\text{-}melt}$ can be empirically estimated by making a quadratic regression between the $\delta^{49}Ti_{OL\text{-}Ti}$ and $\ln\left(f\_Ti\right)$ values of the Hekla samples. While the temperatures during fractional crystallization of Fe-Ti oxides can be estimated by calculating liquidus temperatures of the samples using rhyolite-MELTS (*50*) with an assumed pre-eruptive $H_2O/K_2O \approx 2$ and a pressure of 2000 bars (*30*), we can compare the $\Delta^{49}Ti_{crystal\text{-}melt}$ values with the temperatures of fractional crystallization. Normally, the $\alpha^{49/47}_{crystal\text{-}melt\_i\_or\_j}$ should vary as a function of temperature (T in K) according to:

$$\alpha^{49/47}_{crystal\text{-}melt\_i\_or\_j} \approx A \times 10^6 / T^2_{melt\_i\_or\_j} + B \quad \text{(Eq. 7)}.$$

Thus, there should be a linear correlation between the $\Delta^{49}Ti_{crystal\text{-}melt}$ and $10^6 / T^2_{melt}$ values if $\alpha^{49/47}_{crystal\text{-}melt\_i\_or\_j}$ is only temperature-dependent. However, this is not the case for the Hekla samples, and the coefficients A and B in Equation 7 are not constant. As shown in the inset of Fig. S1, the $\Delta^{49}Ti_{crystal\text{-}melt}$ value is increasing with higher $10^6 / T^2_{melt}$ values, but the increase on the $\Delta^{49}Ti_{crystal\text{-}melt}$ value gradually slows down when $10^6 / T^2_{melt}$ values are higher. This observation implies that the $\Delta^{49}Ti_{crystal\text{-}melt}$ may be not only controlled by the change in temperature but also the change in melt structure, i.e., the stronger melt polymerization with increasing SiO_2 contents that leads to an increase in the fractions of 5- and 4-folded coordinated Ti in the silicate melts (*49*) and enlarges the $\Delta^{49}Ti_{crystal\text{-}melt}$ factor. By comparison with the Hekla lavas, the pre-erupted temperatures of the Afar magmas cannot be well estimated yet due to the lack of information on their pre-erupted H_2O contents. However, the similar $\delta^{49}Ti$-SiO_2

paths between the Afar and Hekla samples suggest that Ti isotopes behave similarly in these two igneous suites.

The basaltic to andesitic samples of Agung volcano from Sunda Arc (Dataset S5) (*19*) in (*17*) define a $\Delta^{49}Ti_{crystal-melt}$ value of −0.16 ± 0.01 ‰ (inset in Fig. S1), while the Hekla samples with SiO_2 = 46.5-58.1 wt% show an average value of −0.20 ± 0.01 ‰ (Fig. S1). The $\Delta^{49}Ti_{crystal-melt}$ value provided by the Agung samples agrees with those obtained from the Hekla samples if the Agung H_2O/K_2O ratio is ≈ 0 (i.e., $10^6/T^2$ = 0.45-0.49), while it would be slightly lower for H_2O/K_2O = 1 or 2 (i.e., $10^6/T^2$ = 0.48-0.61 or 0.51-0.65, respectively) (see the inset in Fig. S1). This can be probably related to an earlier degassing of H_2O for the Agung volcano due to a shallower magma storage (≈ 1.9 km) (*33*) compared to that of the Hekla volcano (≈ 6-7 km) (*30*, *32*). Alternatively, this small discrepancy in Ti isotopic fractionation could also be due to the fact that in Agung volcano the major Ti-bearing phase fractionated from the melt is titanomagnetite instead of ilmenite in Hekla volcano (Fig. 2A), due to the difference in chemical composition and oxidation state between island arc magmas (calc-alkaline and oxidized) and plume magmas (tholeiitic and reduced).

Despite this slight uncertainty on the Ti-bearing phases fractionated in the various geodynamical settings, it is clear that, at a given SiO_2 content, lavas from plumes show higher $\delta^{49}Ti$ values than those from island arcs (Fig. 2B). This isotopic difference is likely the sum of two effects: (i) the lower fO_2 in plume magmas delays the saturation of ilmenite or titanomagnetite, and allows the enrichments of TiO_2 in magmas during olivine and plagioclase accumulation (see the inset in Fig. 1A) (*12*, *18*), and (ii) the higher initial TiO_2 contents in plume magmas allow larger magnitude of depletions of Ti by fractional crystallization of Fe-Ti oxides (Fig. 2A) (*13*).

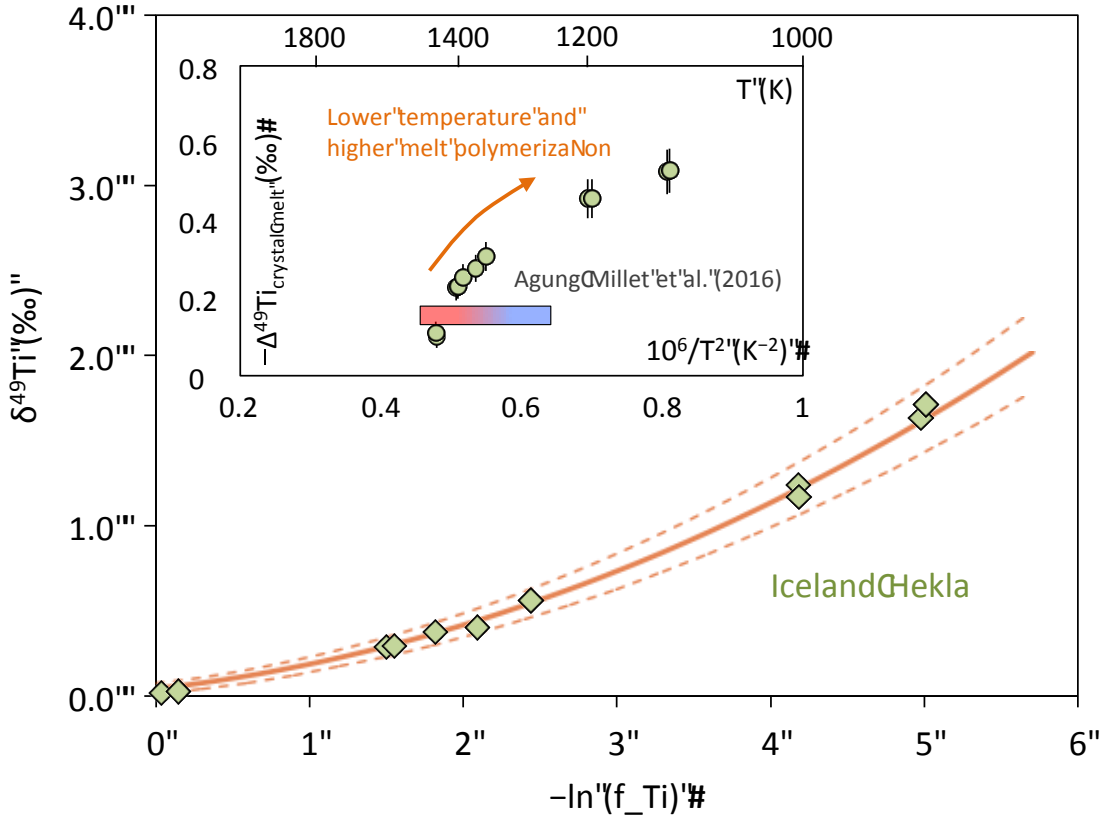

Fig. S1. The correlation between $\delta^{49}Ti$ and $-\ln\left(f\_Ti\right)$ for the Hekla samples. The dashed orange envelope represents the 95 % confidence interval for the regression. The derivation of the quadratic relation between the $\delta^{49}Ti$ and $\ln\left(f\_Ti\right)$ values of the Hekla samples can further provide the instant $\Delta^{49}Ti_{crystal-melt}$ values. The inset shows the relation between the instant $\Delta^{49}Ti_{crystal-melt}$ and $10^6/T^2$ values. The $\Delta^{49}Ti_{crystal-melt}$ value of −0.16 ± 0.01‰ for the Agung basaltic to andesitic samples in (*17*) can be compared with those of the Hekla samples in the inset by using the pre-eruptive H_2O/K_2O ratios of 0 to 2 illustrated by the red to blue change in the colored bar.

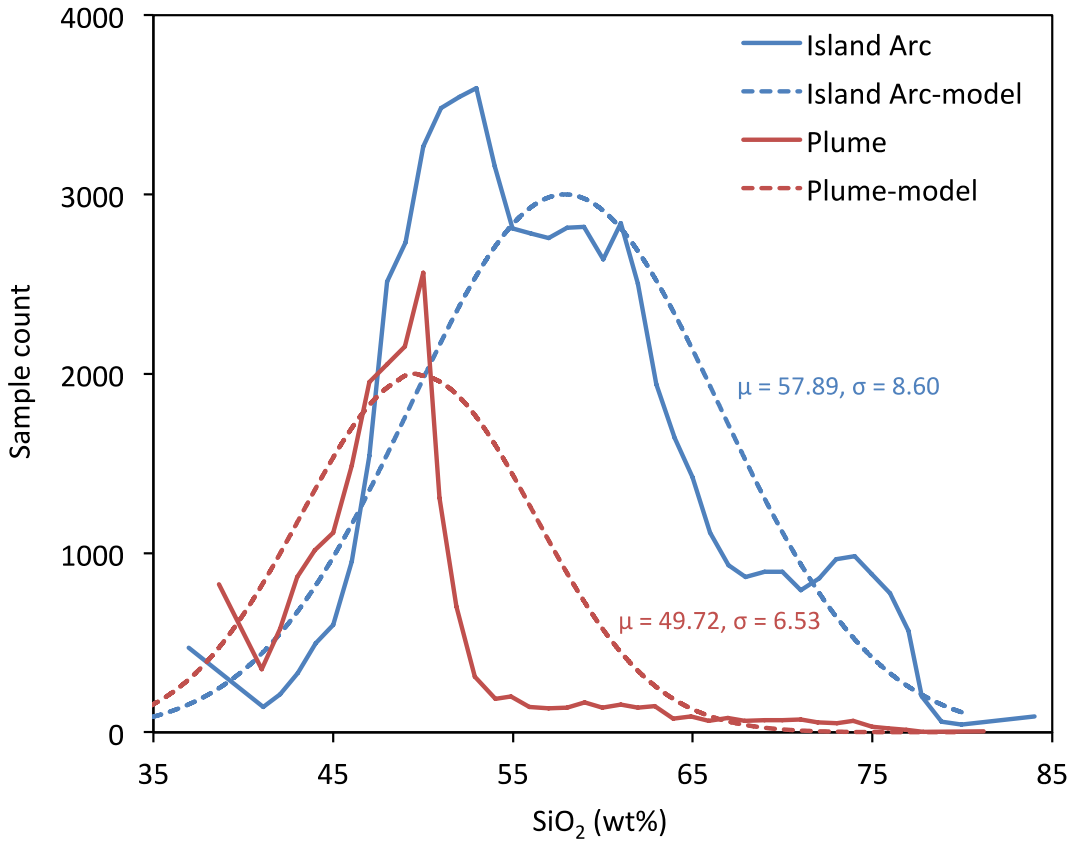

Fig. S2. The SiO_2 distributions for the rocks from plume and island arc settings (the GeoRoc database). Note that some samples may be over-counted due to the non-random sampling, and the SiO_2 distributions for either plume or island arc setting may not strictly follow Gaussian distribution. The use of Gaussian distribution to fit with the dataset provides μ = 49.72 and σ = 6.53 for the rocks from plume settings (n = 44,089) while μ = 57.89 and σ = 8.60 for those from island arc settings (n = 103,090).

References

1. Greber ND *et al.* (2017) Titanium isotopic evidence for felsic crust and plate tectonics 3.5 billion years ago. *Science* **357**: 1271–1274. doi: 10.1126/science.aan8086
2. Korenaga J (2013) Initiation and evolution of plate tectonics on Earth: theories and observations. *Annu. Rev. Earth Planet. Sci.* **41**: 117–151. doi: 10.1146/annurev-earth-050212-124208
3. Watson EB, Harrison TM (2005) Zircon thermometer reveals minimum melting conditions on earliest Earth. *Science* **308**: 841–844. doi: 10.1126/science.1110873
4. Martin H (1986) Effect of steeper Archean geothermal gradient on geochemistry of subduction-zone magmas. *Geology* **14**: 753–756. doi: 10.1130/0091-7613(1986)14<753:EOSAGG>2.0.CO;2
5. Dhuime B, Wuestefeld A, Hawkesworth CJ (2015) Emergence of modern continental crust about 3 billion years ago. *Nat. Geosci.* **8**: 552–555. doi: 10.1038/ngeo2466
6. Tang M, Chen K, Rudnick RL (2016) Archean upper crust transition from mafic to felsic marks the onset of plate tectonics. *Science* **351**: 372–375. doi: 10.1126/science.aad5513
7. Harrison TM, Bell EA and Boehnke P (2017) Hadean zircon petrochronology. *Rev. Mineral. Geochem.* **83**: 329–363. doi: 10.2138/rmg.2017.83.11
8. Boehnke P, Bell EA, Stephan T, Trappitsch R, Keller CB, Pardo OS, Davis AM, Harrison TM, Pellin MJ (2018) Potassic, high-silica Hadean crust. *Proc. Natl. Acad. Sci. USA*, p.201720880. doi: 10.1073/pnas.1720880115
9. Campbell IH, Davies DR (2017) Raising the continental crust. *Earth Planet. Sci. Lett.* **460**: 112–122. doi: 10.1016/j.epsl.2016.12.011
10. Reimink JR, Chacko T, Stern RA, Heaman LM (2014) Earth's earliest evolved crust generated in an Iceland-like setting. *Nat. Geosci.* **7**: 529–533. doi: 10.1038/ngeo2170
11. Willbold M, Hegner E, Stracke A, Rocholl A (2009) Continental geochemical signatures in dacites from Iceland and implications for models of early Archaean crust formation. *Earth Planet. Sci. Lett.* **279**: 44–52. doi: 10.1016/j.epsl.2008.12.029
12. Toplis MJ, Carroll MR (1995) An experimental study of the influence of oxygen fugacity on Fe-Ti oxide stability, phase relations, and mineral-melt equilibria in ferro-basaltic systems. *J. Petrol.* **36**: 1137–1170. doi: 10.1093/petrology/36.5.1137
13. Cawthorn RG, Biggar GM (1993) Crystallization of titaniferous chromite, magnesian ilmenite and armalcolite in tholeiitic suites in the Karoo Igneous Province. *Contrib. Mineral. Petrol.* **114**: 221–235. doi: 10.1007/BF00307757
14. Nandedkar RH, Ulmer P, Müntener O (2014) Fractional crystallization of primitive, hydrous arc magmas: an experimental study at 0.7 GPa. *Contrib. Mineral. Petrol.* **167**: 1015. doi: 10.1007/s00410-014-1015-5
15. Savage PS, Georg RB, Williams HM, Burton KW, Halliday AN (2011) Silicon isotope fractionation during magmatic differentiation. *Geochim. Cosmochim. Acta*. **75**: 6124–6139. doi: 10.1016/j.gca.2011.07.043
16. Pik R, Marty B, Hilton DR (2005) How many mantle plumes in Africa? The

geochemical point of view. *Chem. Geol.* **226**: 100–114. doi: 10.1016/j.chemgeo.2005.09.016
17. Millet MA, Dauphas N, Greber ND, Burton KW, Dale CW, Debret B, Macpherson CG, Nowell GM, Williams HM (2016) Titanium stable isotope investigation of magmatic processes on the Earth and Moon. *Earth Planet. Sci. Lett.* **449**: 197–205. doi: 10.1016/j.epsl.2016.05.039
18. Prytulak J, Elliott T (2007) TiO_2 enrichment in ocean island basalts. *Earth Planet. Sci. Lett.* **263**: 388–403. doi: 10.1016/j.epsl.2007.09.015
19. Dempsey S (2013) Geochemistry of volcanic rocks from the Sunda Arc. *Doctoral thesis*, Durham University.
20. Keller CB, Schoene B (2012) Statistical geochemistry reveals disruption in secular lithospheric evolution about 2.5 Gyr ago. *Nature* **485**: 490–493. doi: 10.1038/nature11024
21. Deng Z, Moynier F, Sossi PA, Chaussidon M (in press) Bridging the depleted MORB mantle and the continental crust using titanium isotopes. *Geochem. Perspect. Lett.*
22. Rudnick RL, Gao S (2003) Composition of the continental crust. *Treatise on Geochemistry* **3**: 659. doi: 10.1016/B0-08-043751-6/03016-4
23. Deng Z, Moynier F, van Zuilen K, Sossi PA, Pringle EA, Chaussidon M (2018) Lack of resolvable titanium stable isotopic variations in bulk chondrites. *Geochim. Cosmochim. Acta*. **239**: 409–419. doi: 10.1016/j.gca.2018.06.016
24. Zhang J, Dauphas N, Davis AM, Pourmand A (2011) A new method for MC-ICPMS measurement of titanium isotopic composition: Identification of correlated isotope anomalies in meteorites. *J. Anal. At. Spectrom.* **26**: 2197–2205. doi: 10.1039/C1JA10181A
25. Creech JB, Paul B (2015) IsoSpike: Improved Double‐Spike Inversion Software. *Geostand. Geoanal. Res.* **39**: 7–15. doi: 10.1111/ j.1751-908X.2014.00276.x
26. Yang J, Siebert C, Barling J, Savage P, Liang YH, Halliday AN (2015) Absence of molybdenum isotope fractionation during magmatic differentiation at Hekla volcano, Iceland. *Geochim. Cosmochim. Acta.* **162**: 126–136. doi: 10.1016/j.gca.2015.04.011
27. Chen H, Savage PS, Teng FZ, Helz RT, Moynier F (2013) Zinc isotope fractionation during magmatic differentiation and the isotopic composition of the bulk Earth. *Earth Planet. Sci. Lett.* **369–370**: 34–42. doi: 10.1016/j.epsl.2013.02.037
28. Prytulak J, Sossi PA, Halliday AN, Plank T, Savage PS, Woodhead JD (2017) Stable vanadium isotopes as a redox proxy in magmatic systems? *Geochem. Perspect. Lett.* **3**: 75–84. doi: 10.7185/geochemlet.1708
29. Schuessler JA, Schoenberg R, Sigmarsson O (2009) Iron and lithium isotope systematics of the Hekla volcano, Iceland-Evidence for Fe isotope fractionation during magma differentiation. *Chem. Geol.* **258**: 78–91. doi: 10.1016/j.chemgeo.2008.06.021
30. Lucic G, Berg AS, Stix J (2016) Water-rich and volatile-undersaturated magmas at Hekla volcano, Iceland. *Geochem. Geophys. Geosyst.* **17**: 3111–3130. doi: 10.1002/2016GC006336
31. Moune S, Sigmarsson O, Thordarson T, Gauthier PJ (2007) Recent volatile evolution

in the magmatic system of Hekla volcano, Iceland. *Earth Planet. Sci. Lett.* **255**: 373–389. doi: 10.1016/j.epsl.2006.12.024
32. Weber G, Castro JM (2017) Phase petrology reveals shallow magma storage prior to large explosive silicic eruptions at Hekla volcano, Iceland. *Earth Planet. Sci. Lett.* **466**: 168–180. doi: 10.1016/j.epsl.2017.03.015
33. Chaussard E, Amelung F (2012) Precursory inflation of shallow magma reservoirs at west Sunda volcanoes detected by InSAR. *Geophys. Res. Lett.* **39**. doi:10.1029/2012GL053817
34. Dia A, Dupre B, Gariepy C, Allegre CJ (1990) Sm-Nd and trace-element characterization of shales from the Abitibi Belt, Labrador Trough, and Appalachian Belt: consequences for crustal evolution through time. *Can. J. Earth Sci.* **27**: 758–766. doi: 10.1139/e90-077
35. Mojzsis SJ, Arrhenius G, McKeegan KD, Harrison TM, Nutman AP, Friend CRL (1996) Evidence for life on Earth before 3,800 million years ago. *Nature* **384**: 55–59. doi: 10.1038/384055a0
36. Nutman AP, McGregor VR, Friend CRL, Bennett VC, Kinny PD (1996) The Itsaq Gneiss Complex of southern West Greenland; the world's most extensive record of early crustal evolution (3900-3600 Ma). *Precambrian Res.* **78**: 1–39. doi: 10.1016/0301-9268(95)00066-6
37. Krüner A, Byerly GR, Lowe DR (1991) Chronology of early Archaean granite-greenstone evolution in the Barberton Mountain Land, South Africa, based on precise dating by single zircon evaporation. *Earth Planet. Sci. Lett.* **103**: 41–54. doi: 10.1016/0012-821X(91)90148-B
38. Schopf JW (1983) Earth's earliest biosphere: its origin and evolution. Princeton University Press, Princeton, NJ, USA.
39. Pidgeon RT (1978) 3450-m.y.-old volcanics in the Archaean layered greenstone succession of the Pilbara Block, Western Australia. *Earth Planet. Sci. Lett.* **37**: 421–428. doi: 10.1016/0012-821X(78)90057-2
40. Beaumont V, Robert F (1999) Nitrogen isotope ratios of kerogens in Precambrian cherts: A record of the evolution of atmosphere chemistry? *Precambrian Res.* **96**: 63–82. doi: 10.1016/S0301-9268(99)00005-4
41. Jahn B, Bertrand-Sarfati J, Morin N, Mace J (1990) Direct dating of stromatolitic carbonates from the Schmidtsdrif Formation (Transvaal Dolomite), South Africa, with implications on the age of the Ventersdorp Supergroup. *Geology* **18**: 1211–1214. doi: 10.1130/0091-7613(1990)018<1211:DDOSCF>2.3.CO;2
42. Karhu J, Epstein S (1986) The implication of the oxygen isotope records in coexisting cherts and phosphates. *Geochim. Cosmochim. Acta.* **50**: 1745–1756. doi: 10.1016/0016-7037(86)90136-5
43. Bolhar R, Hofmann A, Woodhead J, Hergt J, Dirks P (2002) Pb- and Nd-isotope systematics of stromatolitic limestones from the 2.7 Ga Ngezi group of the Belingwe Greenstone Belt: Constraints on timing of deposition and provenance. *Precambrian Res.* **114**: 277–294. doi: 10.1016/S0301-9268(01)00229-7
44. Pringle EA, Savage PS, Jackson MG, Barrat JA, Moynier F (2013) Si isotope homogeneity of the solar nebula. *Astrophys. J.* **779**.

doi:10.1088/0004-637X/779/2/123.
45. Rudge JF, Reynolds BC, Bourdon B (2009) The double spike toolbox. *Chem. Geol.* **265**: 420–431. doi: 10.1016/j.chemgeo.2009.05.010
46. de Laeter JR, Böhlke JK, De Bièvre P, Hidaka H, Peiser HS, Rosman KJR, Taylor PDP (2003) Atomic weights of the elements. Review 2000 (IUPAC Technical Report). *Pure Appl. Chem.* **75**, doi:10.1351/pac200375060683.
47. Williams N. H. (2014) Titanium isotope cosmochemistry. Ph.D. thesis, Manchester Univ.
48. Papike JJ, Karner JM, Shearer CK (2005) Comparative planetary mineralogy: Valence state partitioning of Cr, Fe, Ti, and V among crystallographic sites in olivine, pyroxene, and spinel from planetary basalts. *Am. Mineral.* **90**: 277–290. doi: 10.2138/am.2005.1779
49. Farges F, Brown GE (1997) Coordination chemistry of titanium(IV) in silicate glasses and melts: IV. XANES studies of synthetic and natural volcanic glasses and tektites at ambient temperature and pressure. *Geochim. Cosmochim. Acta.* **61**: 1863–1870. doi: 10.1016/S0016-7037(97)00050-1
50. Gualda GAR, Ghiorso MS, Lemons RV, Carley TL (2012) Rhyolite-MELTS: A modified calibration of MELTS optimized for silica-rich, fluid-bearing magmatic systems. *J. Petrol.* **53**: 875–890. doi: 10.1093/petrology/egr080